Sun, M., et al., 2022, Stagnation and tearing of the subducting northwest Pacific slab: Geology, v. 50, https://doi.org/10.1130/G49862.1

Supplemental Material

Stagnation and tearing of the subducting northwest Pacific slab

Muchen Sun[1], Youqiang Yu[1*], Stephen S. Gao[2] and Kelly H. Liu[2]

[1]State Key Laboratory of Marine Geology, Tongji University, Shanghai 200092, China. Email: yuyouqiang@tongji.edu.cn

[2]Geology and Geophysics Program, Missouri University of Science and Technology, Rolla, MO 65409, USA

**Corresponding author: Youqiang Yu (yuyouqiang@tongji.edu.cn)*

Introduction

This document contains detailed descriptions of the data and methods utilized to obtain the results presented in the paper, as well as Supplementary Figure DR1 and Table DR1. This material is associated with Sun et al., ***Slab stagnation and tearing of the subducting Northwest Pacific plate.***

Data

All the broadband seismic data used in this study were obtained from the Data Management Center (DMC) of the Incorporated Research Institutions for Seismology (IRIS; https://ds.iris.edu/ds/nodes/dmc) and the Data Management Center of China National Seismic Network at Institute of Geophysics, China Earthquake Administration (SEISDMC; http://www.seisdmc.ac.cn; Zheng et al., 2010). We requested all the available three-component broadband teleseismic data recorded by 381 stations in the area (120°E to 145°E, and 29°N to 50°N), which is slightly larger than our study area (125°E to 145°E, and 30°N to 48°N), to ensure the reliability of the results at the edges. The recording duration of these seismic data is from mid-1986 to January-2021. To achieve an optimal balance between the quality and quantity of the requested data, an empirical equation of the variable cutoff magnitude (M_c) was used, which can be expressed as $M_c=5.2 + (\Delta - 30.0)/(180.0 - 30.0) - D/700.0$. Here, the Δ represents the epicentral distance ranging from 30° to 100°, while the D is focal depth in kilometer.

Method

All the details about the data processing procedure, including data selection, pre-processing, moveout correction, and stacking under a non-plane-wave assumption, are similar to those in the previous study for the contiguous United States (Gao and Liu, 2014a). We applied a four-pole, two-pass bandpass Bessel filter with corner frequencies 0.02 and 0.2 Hz to keep the low-frequency signals and enhance the signal-to-noise ratio (SNR) of the seismograms. Then the SNR-based procedures (Gao and Liu, 2014a) were utilized to reject seismograms with the P-wave first-arrival SNR on the vertical component less than 4.0. The SNR is defined as max |As| ／ |Ān|, where max |As| is the maximum absolute amplitude on the vertical seismogram 8 s before and 17 s after the predicted IASP91 arrival time for the first P-wave, and |Ān| is the mean absolute amplitude in the time window of 10–20 s before the predicted P-wave arrival time. Following the deconvolution procedure of Ammon (1991), all the filtered high-quality seismograms were converted into the radial receiver functions (RFs). To further improve the accuracy of the resulting RFs, we visually verified to remove the ones with abnormal arrivals or no clear first P pulse. After all these processes, a total of 139,740 RFs from 9,870 events were finally selected for the RF investigation.

Before stacking the RFs, the IASP91 Earth model was employed to ray-trace the path of the converted phase (Pds) and calculate the theoretical coordinates of the ray-piercing points at the middle of the MTZ (535 km). Then we stacked all the RFs with piercing points in each of the radius=1° circular bins to generate a depth series. Considering the size of the first Fresnel zone of shear waves at the MTZ depth, the distance between the centers of adjacent bins is set to 1°, and therefore, there is an overlap among neighboring bins. Bins with less than 8 RFs were not used. The mean and standard deviation of the MTZ discontinuity depths and MTZ thickness in each bin were determined following a bootstrap resampling procedure with 50 resampling iterations (Efron and Tibshirani, 1986). For each bootstrap iteration,1-1/e=63% independent RFs were chosen randomly. About 60% of the chosen ones were then duplicated so that the total number of the new set of RFs is the same as that of the original set. The depths of the d410 and d660 were obtained by picking the maximum stacking amplitude on the resulting depth series in a predefined depth window, which ranges from 380 to 440 km for the d410, and from 630 to 690 km for the d660 with a vertical grid size of 1 km. For a small portion of the traces that have multiple arrivals with comparable amplitudes (e.g., Figure DR1) that might be caused by the P-

to-S conversions from the subducted slab boundaries in the possible ranges of MTZ discontinuities, the depth window was adjusted by considering the recent seismic tomography results in the upper mantle and MTZ, and the determined depth in the neighboring bins.

Since the RFs were moveout-corrected utilizing the 1-D IASP91 Earth model, the resulting MTZ discontinuity depths are apparent rather than true depths. To reliably convert the apparent depths into true depths, well-determined 3-D velocity models for both Vp and Vs with sufficient spatial resolution for the crust, upper mantle, and MTZ, are required. In this study we use TX2019slab, which is a global Vp and Vs model (Lu et al., 2019), to conduct velocity corrections based on the procedure proposed by Gao and Liu (2014b). To perform the correction, the velocity anomalies are smoothed using the cubic B-spline function, and the average P- and S-wave velocities are calculated in radius =1° cylinders with a 10 km thickness for the depth range of 0–700 km. Lastly, we convert the apparent depths (H_A) into the true depths (H_T) using the equation $H_T = \frac{(V_{s0}+\delta V_s)\times(V_{p0}+\delta V_p)}{V_{p0}+\delta V_p - V_{s0}-\delta V_s} \times \frac{V_{p0}-V_{s0}}{V_{p0}\times V_{s0}} H_A$, where V_{p0} and V_{s0} are the mean P- and S-velocity in the layer in the standard Earth model, and δV_p and δV_s are the absolute P- and S-wave velocity anomalies. The spatially continuous images of the discontinuity depths and MTZ thickness were obtained using a continuous curvature surface gridding algorithm with a tension factor of 0.5 (Smith and Wessel, 1990).

Supplemental References

Ammon, C.J., 1991. The isolation of receiver effects from teleseismic P waveforms. Bulletin-Seismological Society of America, v. 81, p. 2504-2510.

Chen, C., Zhao, D., Tian, Y., Wu, S., Hasegawa, A., Lei, J., Park, J.H. and Kang, I.B., 2017. Mantle transition zone, stagnant slab and intraplate volcanism in Northeast Asia. Geophysical Journal International, v. 209, p. 68-85. https://doi.org/10.1093/gji/ggw491.

Efron, B. and Tibshirani, R., 1986. Bootstrap methods for standard errors, confidence intervals, and other measures of statistical accuracy. Statistical science, p. 54-75. https://doi.org/10.1016/j.epsl.2018.09.012.

Gao, S.S. and Liu, K.H., 2014a. Mantle transition zone discontinuities beneath the contiguous United States. Journal of Geophysical Research: Solid Earth, v. 119, p. 6452-6468. https://doi.org/10.1002/2014JB011253

Gao, S.S. and Liu, K.H., 2014b. Imaging mantle discontinuities using multiply-reflected P-to-S conversions. Earth and Planetary Science Letters, v. 402, p. 99-106. https://doi.org/10.1016/j.epsl.2013.08.025.

Lu, C., Grand, S.P., Lai, H. and Garnero, E.J., 2019. TX2019slab: A new P and S tomography model incorporating subducting slabs. Journal of Geophysical Research: Solid Earth, v. 124, p. 11549-11567. https://doi.org/10.1029/2019JB017448.

Smith, W.H.F. and Wessel, P., 1990. Gridding with continuous curvature splines in tension. Geophysics, v. 55, p. 293-305. https://doi.org/10.1190/1.1442837.

Zheng, X.F., Yao, Z.X., Liang, J.H., and Zheng, J., 2010. The role played and opportunities provided by IGP DMC of China National Seismic Network in Wenchuan earthquake disaster relief and researches. Bulletin of the Seismological Society of America, v. 100, p. 2866–2872. https://doi.org/10.1785/0120090257.

Supplementary Figure and Table

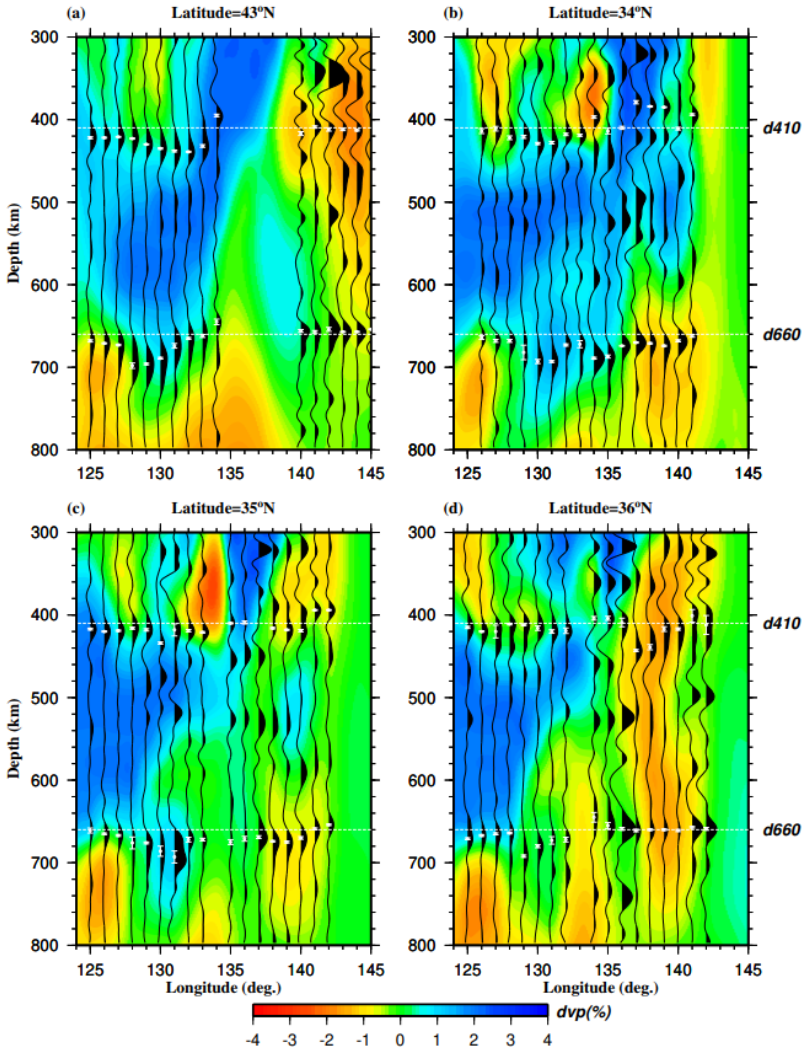

Figure S1. (a) Stacked receiver functions along 43°N latitude with the picked MTZ discontinuity peaks (white dots with error bars). (b), (c) and (d) are same as (a) but for the 34°N, 35°N and 36°N, respectively. The background image shows P-wave velocity anomalies (Chen et al., 2017).

Table S1. Results of receiver function stacking for each bin. The columns are:

clon: longitude of the circle's center

clat: latitude of the circle's center

d410: depth of the d410 (km)

d410_SD: Standard deviation of the d410 depth (km)

d660: depth of the d660 (km)

d660_SD: Standard deviation of the d660 depth (km)

MTZ: Mantle Transition Zone thickness (km)

cd410: depth of the d410 corrected by TX2019slab model (km)

cd660: depth of the d660 corrected by TX2019slab model (km)

cMTZ: Mantle Transition Zone thickness corrected by TX2019slab (km)

Note that a value of zero is given to the depth if the Pds arrival is not well-defined.

clon	clat	d410	d410_SD	d660	d660_SD	MTZ	cd410	cd660	cMTZ
125	48	404	0.9	674	0.6	269	407	680	273
125	47	407	0.5	673	0.7	265	409	678	269
126	48	408	1.0	674	0.9	266	410	679	269
125	46	412	1.0	667	1.1	254	414	671	257
126	47	411	0.9	676	0.8	265	413	681	268
127	48	413	1.0	673	0.7	260	414	678	263
125	45	419	1.5	660	0.8	240	420	664	244
126	46	417	0.8	670	1.1	252	418	674	256
127	47	415	0.6	678	0.8	262	416	681	266
125	44	411	1.1	664	1.0	253	411	668	256
128	48	415	0.7	673	0.7	257	415	677	262
126	45	422	0.9	666	1.4	244	422	669	247
127	46	419	1.4	682	1.7	263	419	685	266
125	43	422	1.2	668	1.4	246	422	672	250
128	47	417	0.7	675	0.6	257	416	678	261
129	48	418	1.2	669	1.1	250	416	672	255
126	44	414	0.9	666	0.9	252	414	669	255
127	45	417	0.7	674	2.3	256	416	676	260
125	42	415	0.5	667	0.8	251	414	670	256
128	46	418	0.5	678	0.9	260	417	680	263
129	47	418	0.7	673	0.5	254	416	675	259
130	48	415	1.7	663	2.0	247	412	665	253
126	43	422	0.6	671	0.6	248	421	674	253

127	44	416	0.8	673	1.3	257	415	675	260
125	41	412	0.5	664	0.7	251	409	666	257
128	45	417	0.7	683	1.2	266	415	684	269
129	46	419	0.7	675	0.7	256	417	677	260
130	47	416	0.6	666	1.0	249	413	668	255
131	48	421	3.9	662	1.8	240	417	663	246
126	42	419	0.9	670	0.6	251	417	672	255
127	43	421	0.6	673	0.9	252	419	675	256
128	44	417	1.2	691	1.4	273	415	692	278
125	40	413	0.4	661	0.5	247	409	662	253
129	45	417	0.4	679	0.8	261	414	680	266
130	46	419	0.5	669	0.6	250	416	671	255
132	48	430	2.1	664	2.2	233	425	664	239
131	47	412	0.5	663	0.6	250	408	665	257
126	41	416	0.8	670	0.7	253	413	671	259
127	42	422	0.7	670	0.5	248	419	672	252
128	43	423	0.7	698	3.3	275	420	699	279
125	39	416	0.7	662	0.2	245	412	663	252
129	44	418	0.8	690	1.6	272	415	692	277
133	48	422	1.9	668	1.2	246	416	668	252
130	45	418	0.5	669	0.4	251	414	670	256
132	47	411	0.7	663	0.7	251	406	664	258
131	46	418	0.6	664	0.5	246	414	666	252
126	40	427	4.7	666	0.8	238	423	667	244
127	41	424	0.8	671	0.5	246	421	672	251
128	42	425	0.5	701	1.3	276	421	702	280
125	38	421	0.7	665	1.0	243	416	666	250
134	48	418	1.0	668	1.3	249	412	668	256
129	43	430	0.5	696	1.0	266	426	697	271
133	47	414	0.9	664	1.0	249	408	665	257
130	44	419	0.7	677	0.9	257	415	678	264
132	46	418	0.8	664	0.4	245	413	666	253
131	45	421	0.6	666	0.2	245	417	667	251
126	39	428	2.8	663	0.5	235	423	664	240
127	40	426	0.9	669	0.7	243	422	669	248
135	48	416	1.3	669	1.5	253	411	670	259
128	41	429	0.5	691	1.4	261	425	691	266
134	47	419	1.5	664	1.1	245	413	666	253
125	37	418	1.7	674	1.2	256	412	674	262
129	42	427	0.6	703	0.9	275	423	703	281
133	46	420	0.5	664	0.4	244	415	666	251

130	43	435	0.8	689	1.0	254	430	690	260
132	45	423	0.5	665	0.5	242	418	666	248
131	44	424	0.9	668	0.6	243	419	669	250
126	38	423	1.2	671	0.7	247	418	671	254
136	48	413	1.4	674	1.8	261	408	675	267
127	39	427	2.1	665	0.9	238	422	665	243
135	47	416	1.3	662	1.7	246	411	664	253
128	40	428	0.8	671	0.9	243	423	670	248
134	46	421	4.5	664	0.9	242	416	665	248
125	36	415	1.3	671	1.2	255	408	670	262
133	45	422	0.8	665	0.5	242	417	667	250
129	41	429	0.6	696	1.1	266	424	696	272
132	44	425	1.1	666	0.5	241	420	667	247
130	42	432	1.1	702	1.5	270	427	702	275
131	43	438	1.1	674	2.8	236	433	675	242
137	48	420	3.7	673	2.2	253	416	675	259
126	37	419	2.6	677	4.1	257	412	677	264
136	47	418	2.5	666	1.3	247	414	669	255
127	38	416	5.6	685	4.0	268	410	685	275
135	46	438	1.6	664	2.5	226	434	665	230
134	45	418	1.8	665	0.7	247	413	666	253
128	39	427	1.4	661	1.2	234	421	661	239
133	44	425	0.6	666	0.7	240	419	667	248
125	35	417	1.1	661	3.1	244	409	660	250
129	40	432	0.6	686	4.8	253	426	686	259
132	43	439	0.6	665	1.1	225	433	665	232
130	41	427	0.6	694	0.8	266	421	693	272
131	42	419	1.0	667	1.6	247	413	667	254
137	47	437	4.1	663	3.4	226	434	667	233
126	36	420	0.8	667	1.1	247	413	666	253
136	46	434	5.0	657	5.4	223	432	659	227
139	48	411	1.9	654	3.0	242	408	656	248
135	45	414	3.8	670	3.2	256	411	671	261
127	37	0	0.0	664	0.6	0	0	663	0
134	44	415	1.2	668	1.1	252	410	668	259
128	38	413	7.4	657	1.2	244	406	656	250
133	43	432	1.6	662	1.8	229	426	663	236
129	39	416	4.3	661	2.9	245	410	661	251
132	42	419	7.7	660	1.4	240	412	659	247
130	40	433	2.1	683	6.6	249	427	682	256
131	41	421	1.1	674	1.7	253	414	673	258

140	48	415	4.3	660	0.0	244	412	663	250
136	45	430	1.4	663	5.5	233	429	666	237
126	35	420	0.8	665	0.9	245	412	663	251
139	47	413	6.1	656	1.5	242	411	662	251
135	44	422	4.6	678	1.7	256	419	679	260
127	36	420	7.8	665	1.2	245	412	663	251
141	48	414	3.3	654	1.5	239	411	658	247
134	43	395	1.5	645	3.3	249	389	645	256
128	37	410	1.0	664	0.9	254	403	663	260
133	42	436	2.0	655	2.6	218	430	654	225
129	38	413	4.7	659	0.8	246	406	659	253
132	41	423	6.4	664	3.7	241	416	662	246
130	39	430	2.6	663	2.1	233	423	663	239
131	40	422	1.9	670	1.6	248	415	668	253
140	47	417	2.9	655	1.1	237	416	661	246
142	48	395	6.7	651	1.6	255	392	655	263
139	46	419	7.5	660	1.1	241	420	667	247
126	34	414	2.9	664	2.3	249	406	662	256
141	47	418	2.0	659	1.2	241	417	666	249
127	35	419	0.8	667	1.1	247	410	665	254
143	48	0	0.0	649	2.1	0	0	652	0
128	36	411	0.9	664	1.0	252	403	662	259
133	41	416	2.4	670	5.8	253	409	669	260
132	40	415	2.2	660	3.7	245	408	658	250
129	37	414	1.2	663	0.9	249	407	663	256
140	46	424	1.5	667	1.1	243	427	675	249
130	38	418	2.1	665	2.8	247	411	665	254
125	32	404	1.4	665	3.6	261	396	663	267
142	47	398	4.3	653	2.1	254	396	659	263
144	48	414	4.0	649	1.1	235	410	652	242
139	45	412	3.1	685	2.1	273	414	692	278
141	46	419	1.3	671	2.1	252	422	680	258
145	48	415	2.8	653	1.8	238	412	657	245
143	47	432	2.2	657	3.9	224	432	663	231
127	34	411	2.8	668	1.8	256	402	666	263
128	35	416	1.2	676	7.2	260	407	674	266
140	45	419	2.0	667	5.6	247	422	675	253
129	36	412	0.8	692	1.4	279	404	692	288
131	38	434	3.3	662	2.1	227	427	662	235
130	37	418	2.6	673	3.4	254	411	674	263
142	46	420	0.9	671	1.2	250	423	680	257

144	47	428	1.0	653	1.0	225	428	659	231
139	44	444	1.3	682	5.7	237	446	688	242
141	45	419	1.7	675	2.7	255	423	684	261
145	47	429	3.3	660	4.0	231	431	667	236
143	46	422	0.5	654	0.7	232	425	662	237
127	33	429	2.9	677	4.3	247	421	675	254
140	44	443	1.2	685	3.8	242	447	693	246
128	34	422	2.3	668	1.7	246	414	666	252
129	35	418	1.4	676	1.1	258	410	675	265
131	37	423	1.6	712	2.3	289	416	713	298
142	45	418	1.0	667	4.9	248	422	676	254
130	36	416	2.7	680	1.8	264	408	681	273
144	46	422	0.5	653	0.6	230	426	661	235
125	30	405	1.6	684	5.3	279	398	683	285
141	44	438	9.4	685	5.1	247	443	694	251
145	46	421	0.5	651	0.6	229	426	660	234
143	45	418	0.7	655	1.3	237	423	664	241
140	43	417	2.3	656	1.7	239	421	664	243
132	37	420	2.6	710	1.9	289	413	712	299
142	44	398	2.6	656	9.3	258	403	665	262
128	33	426	3.3	668	3.7	242	418	666	248
144	45	421	0.5	654	0.7	232	427	663	237
131	36	420	2.2	673	4.5	253	413	674	261
129	34	421	1.8	682	8.8	261	413	680	268
130	35	434	1.2	686	6.2	251	426	686	260
141	43	409	1.3	657	1.5	248	413	665	252
145	45	416	3.5	671	4.8	255	422	681	259
143	44	400	1.9	662	1.0	262	406	671	266
140	42	411	2.2	668	4.5	256	415	676	261
142	43	412	2.0	654	2.4	242	417	663	245
144	44	401	0.9	656	0.6	255	407	665	258
132	36	419	3.3	672	2.9	252	412	674	262
128	32	411	5.7	668	1.4	256	403	666	263
131	35	418	7.3	693	7.3	274	411	694	283
130	34	429	1.3	693	2.5	263	421	693	271
129	33	414	2.6	678	6.8	263	406	676	270
139	41	0	0.0	661	4.9	0	0	669	0
141	42	409	1.1	660	3.9	251	413	668	255
145	44	0	0.0	661	1.4	0	0	670	0
143	43	412	1.3	657	0.5	244	418	666	248
135	38	420	6.1	678	4.7	257	416	679	263

138	40	419	4.6	664	4.9	244	421	669	248
134	37	0	0.0	665	3.5	0	0	666	0
140	41	417	4.5	680	2.0	262	422	688	266
137	39	0	0.0	680	2.9	0	0	683	0
142	42	409	1.2	658	7.8	249	412	664	252
144	43	413	0.8	657	0.6	244	419	665	246
132	35	419	1.3	672	2.9	252	413	675	261
131	34	428	1.5	693	1.2	264	423	695	272
139	40	0	0.0	662	2.9	0	0	669	0
136	38	423	1.2	677	3.6	254	421	680	258
128	31	402	3.1	649	5.0	247	394	647	253
130	33	423	3.3	686	1.2	262	417	686	269
129	32	421	5.6	675	1.8	254	413	674	260
141	41	391	1.9	0	0.0	0	395	0	0
145	43	0	0.0	654	0.5	0	0	660	0
143	42	413	1.5	664	2.5	250	415	669	254
135	37	422	1.4	644	6.6	222	420	646	227
138	39	410	5.4	679	3.4	268	411	683	272
134	36	404	2.2	645	5.8	241	398	646	248
140	40	413	1.9	663	1.7	250	418	671	253
144	42	415	1.0	663	2.0	248	416	666	250
142	41	395	1.2	0	0.0	0	396	0	0
137	38	422	2.7	683	2.2	261	422	686	265
133	35	421	0.9	672	1.6	251	416	676	260
132	34	418	1.5	673	1.3	254	414	677	262
139	39	407	1.5	661	1.8	253	410	667	257
136	37	421	1.0	649	1.9	227	420	652	232
131	33	432	3.5	687	2.7	254	431	692	261
141	40	399	5.2	656	4.8	256	404	664	260
130	32	414	8.4	677	1.5	263	409	679	270
143	41	395	1.4	0	0.0	0	395	0	0
128	30	404	1.7	648	4.5	244	399	648	249
129	31	404	2.6	674	1.7	270	398	674	277
135	36	404	2.4	655	3.6	250	401	658	257
138	38	431	2.7	669	4.6	237	431	672	241
140	39	409	1.1	662	2.1	252	413	669	256
142	40	399	2.7	655	3.3	256	401	660	259
137	37	425	2.1	659	1.9	233	425	662	238
133	34	419	1.3	672	4.3	253	412	673	261
139	38	412	1.0	661	0.8	248	414	666	252
132	33	402	0.8	683	6.1	280	396	684	288

136	36	409	5.2	659	1.8	250	407	662	255
141	39	406	1.2	657	1.8	251	411	664	254
143	40	403	0.9	654	2.0	250	404	657	253
131	32	419	2.5	679	1.4	260	417	684	267
130	31	413	3.2	684	7.7	270	411	689	278
129	30	406	1.5	643	2.3	237	404	646	243
135	35	410	0.7	675	3.0	265	406	678	272
138	37	424	4.0	660	1.4	236	425	664	239
140	38	410	0.8	659	1.0	248	414	666	252
142	39	406	0.9	654	1.2	247	409	659	250
134	34	397	1.5	689	1.1	291	390	691	301
137	36	443	1.2	661	1.5	218	444	665	221
133	33	402	1.4	689	2.7	286	394	688	294
139	37	415	1.0	661	1.0	245	417	666	249
141	38	410	0.8	658	1.0	248	414	664	251
143	39	401	1.9	652	3.3	251	403	656	253
136	35	409	1.8	671	2.9	262	407	676	268
132	32	413	1.0	683	1.8	269	406	683	276
131	31	412	1.1	685	2.6	273	408	687	280
138	36	439	3.1	660	1.0	221	441	665	224
130	30	410	1.9	676	1.0	265	408	681	273
135	34	414	3.4	687	1.9	272	408	690	281
144	39	407	1.5	0	0.0	0	409	0	0
140	37	412	0.6	661	0.8	248	415	667	252
142	38	408	1.2	651	1.7	242	410	656	245
134	33	398	0.9	683	1.2	285	390	683	293
137	35	0	0.0	669	1.7	0	0	675	0
133	32	415	0.6	685	3.9	270	407	683	276
139	36	417	2.9	660	1.0	243	419	665	246
141	37	407	3.7	656	1.0	249	409	661	252
136	34	410	1.9	674	0.6	264	408	678	270
132	31	414	0.5	684	1.1	269	407	683	277
138	35	416	0.8	674	0.7	258	419	680	262
131	30	405	1.4	664	5.0	258	398	664	266
135	33	415	8.1	682	1.4	266	409	685	275
140	36	417	1.4	661	1.3	243	419	666	247
142	37	410	1.9	656	1.5	245	413	661	248
134	32	419	1.2	705	2.0	286	412	705	293
137	34	379	2.0	670	0.9	290	379	676	298
139	35	418	0.7	675	1.1	257	422	682	260
143	37	404	3.6	0	0.0	0	406	0	0

141	36	401	7.7	657	0.9	255	403	661	259
133	31	416	0.6	683	3.8	266	408	681	273
136	33	408	3.5	674	0.7	265	404	679	275
132	30	404	1.5	662	1.7	257	396	660	264
138	34	384	0.7	671	0.8	286	388	679	292
142	36	412	11.4	659	1.7	247	414	664	250
140	35	419	1.4	670	1.5	251	422	676	254
135	32	418	2.9	681	1.9	262	412	682	270
137	33	421	1.1	670	1.0	248	423	678	255
134	31	412	5.9	704	2.6	291	405	704	299
139	34	385	0.5	674	0.8	289	391	683	293
141	35	394	0.6	659	1.2	265	395	663	268
136	32	416	0.9	0	0.0	0	412	0	0
138	33	423	0.3	0	0.0	0	429	0	0
142	35	394	0.5	654	0.8	259	396	659	263
140	34	411	1.6	668	1.2	257	415	676	260
135	31	423	1.5	704	3.0	281	418	706	288
137	32	421	3.1	0	0.0	0	420	0	0
141	34	394	1.1	662	1.6	267	396	667	272
138	32	420	4.8	698	5.2	277	426	711	285
139	32	424	3.9	703	8.0	279	433	717	285
138	31	402	5.5	695	2.7	293	404	707	303
140	32	431	3.9	677	2.8	246	439	690	251
141	32	431	2.8	677	2.3	246	436	687	251
139	31	396	2.0	694	3.9	298	404	710	307
142	32	434	2.4	678	2.3	243	437	686	249
140	31	416	4.9	656	6.2	239	425	671	246
141	31	426	1.3	674	2.7	248	432	686	254